Alexandria Engineering Journal (2016) 55, 2351–2365

HOSTED BY

Alexandria University

Alexandria Engineering Journal

www.elsevier.com/locate/aej
www.sciencedirect.com

ORIGINAL ARTICLE

Numerical investigation of flow past a row of rectangular rods

S.Ul. Islam [a,*], H. Rahman [a], W.S. Abbasi [a], S.C. Saha [b], T. Shahina [c]

[a] Mathematics Department, COMSATS Institute of Information Technology, Islamabad 44000, Pakistan
[b] School of Chemistry, Physics and Mechanical Engineering, Queensland University of Technology, Brisbane, QLD 4001, Australia
[c] Department of Meteorology, COMSATS Institute of Information Technology, Islamabad 44000, Pakistan

Received 19 November 2014; revised 4 April 2016; accepted 4 May 2016
Available online 1 June 2016

KEYWORDS

Aspect ratio;
Flow patterns;
Force statistics;
Gap spacing;
Lattice Boltzmann method;
Rectangular rods

Abstract A numerical study of uniform flow past a row of rectangular rods with aspect ratio defined as R = width/height = 0.5 is performed using the Lattice Boltzmann method. For this study the Reynolds number (Re) is fixed at 150, while spacings between the rods (g) are taken in the range from 1 to 6. Depending on g, the flow is classified into four patterns: flip-flopping, nearly unsteady-inphase, modulated inphase-antiphase non-synchronized and synchronized. Sudden jumps in physical parameters were observed, attaining either maximum or minimum values, with the change in flow patterns. The mean drag coefficient (Cdmean) of middle rod is higher than the second and fourth rod for flip-flopping pattern while in case of nearly unsteady-inphase the middle rod attains minimum drag coefficient. It is also found that the Strouhal number (St) of first, second and fifth rod decreases as g increases while that of other two have mixed trend. The results further show that there exist secondary interaction frequencies together with primary vortex shedding frequency due to jet in the gap between rods for $1 \leqslant g \leqslant 3$. For the average values of Cdmean and St, an empirical relation is also given as a function of gap spacing. This relation shows that the average values of Cdmean and St approach to those of single rectangular rod with increment in g.

1. Introduction

Bluff structures, for example, circular and rectangular rods are the most common configuration in numerous practical applications. At high Reynolds numbers (Re) these applications can be found in bridges, chimneys, tall buildings, fences, overhead power-line bundles, masts, chemical-reaction towers, etc. Flow around a bluff body often involves various fluid dynamic phenomena, such as reattachment, separation and vortex shedding, while at low Re these applications can be found in micro-devices, such as in micro-electro-mechanical-system (MEMS) and cooling of fibers. Due to these applications the study of bluff body flow gained attractiveness in both science and engineering. Numerous studies have concentrated on flow past a square rod [1–3]. However, much less work has been conducted for a rectangular rod. The flow around a rectangular rod can result various local instabilities which can lead to global instabilities [4]. A small change in aspect ratio (R) can result drastic changes in the fluid dynamic characteristics

* Corresponding author.
E-mail address: islam_shams@comsats.edu.pk (S.Ul. Islam).
Peer review under responsibility of Faculty of Engineering, Alexandria University.

http://dx.doi.org/10.1016/j.aej.2016.05.003

Nomenclature

c_1	first rod
c_2	second rod
c_3	third rod
c_4	fourth rod
c_5	fifth rod
c_s	speed of sound
Cd	drag coefficient
Cl	lift coefficient
Cdmean	mean drag coefficient
Cdrms	root-mean-square value of the drag coefficient
Clrms	root-mean-square value of the lift coefficient
D	space dimension
E	spectrum energy
$\mathbf{e}_i$	particle velocity directions
f_i	particle distribution function
$f_i^{(eq)}$	equilibrium particle distribution function
f_s	vortex shedding frequency
Fd	force component in the in-line direction
Fl	force component in the transverse direction
g	gap spacing between rods
H	height of the computational domain
h	height of the rectangular rods
L	length of the channel
Lu	upstream distance from inlet to five rods
Ld	downstream distance from five rods to outlet boundary
p	pressure
Q	number of particles
Re	Reynolds number
s	surface-to-surface distance between rods
St	Strouhal number
$\mathbf{u}$	macroscopic velocity components
U_∞	uniform inflow velocity
w	width of the rectangular rods
w_i	weighting coefficients
$\mathbf{x}$	position of particle
τ	single-relaxation-time parameter

around the rod [5–7]. Further, the wakes of multiple bluff bodies placed next to each other create complex flow structures which also create instabilities and may cause acoustic noise or structural vibrations, which in some cases can trigger structure failure. Okajima [1] and Islam et al. [7] found that the drag coefficient undergoes significant changes in the range of $R = 0$–1. Abdollah et al. [5] experimentally and Islam et al. [7] numerically observed that the vortex formation region is smaller in the case of small aspect ratio compared to square rod ($R = 1$). Islam et al. [7] also observed that the physical parameters, such as drag coefficient (Cd) and Strouhal number (St) values for $R < 1$ are higher than those at $R = 1$ case. On the basis of above mentioned findings we chose the middle value of R from 0 to 1 in this numerical investigation.

Numerous experimental and numerical studies around two, three and four circular as well as square rods have been widely carried out. In spite of its great relevance to practical engineering problems, the flow past rectangular rods with different aspect ratios has received much less attention. Zdravkovich [8] categorized the flow interference between rods in proximity interference, wake interference and a combination of these two. To cite a few more examples, Sumner et al. [9] examined the wake of two and three side-by-side circular rods in a range of gap spacing (g) from 1 to 6 with $Re = 500$–3000 using particle image velocimetry and hot film anemometry. In their studies, for two rods case, single vortex street flow, deflected gap flow and synchronized vortex shedding, observed as g increased. In case of three rods, symmetric and asymmetric biased flow patterns were observed at $g = 1.25$. Alam and Zhou [10] studied the wake features, gap vortices, flow switch, and merging of two streets into one and also gave the quantitative information for flow around two side-by-side square rods using water tunnel experiment at $Re = 300$. In their investigation, they found four flow patterns, each characterized in terms of wake mechanism and vortex formation length. Agrawal et al. [11] found the inphase and antiphase vortex shedding behind two rods at $g = 3$, and biased flow pattern at $g = 1.7$, at $Re = 73$. Kang [12] investigated the wake of three side-by-side circular rods at a Reynolds number of 100 at $g < 5$. He observed five different kinds of flow patterns: single bluff-body ($g < 0.3$), deflected ($g \approx 0.3$), flip-flopping ($0.3 < g \leqslant 1.2$), inphase synchronized ($g \approx 1.5$) and modulation synchronized patterns ($g \geqslant 2$). The effects of gap spacing and Reynolds number on flow past three side-by-side square rods were investigated by Rahman et al. [13] and Islam et al. [14]. They found that the flow structure is strongly dependent on Reynolds number and gap spacing while the later one is more effective in case of unequal g.

On the other hand, investigations on flow past row of rods (more than three rods) are relatively scarce. In most of the studies emphases were on flow patterns for varying gap spacing in terms of wake structures and experimentally Guillaume and LaRue [15] observed flopping regime for flow past two, three and four rods array. Investigation in terms of physical parameters and time-trace analysis of each rod has not been well documented in the literature. Huang et al. [16] investigated vortex shedding characteristics on flow around row of circular rods, at a Reynolds number of 150, using FLUENT. They found that the vortex streets are stable and keep the same form for large distance at downstream of the computational domain for $g = 4$ and for $g < 2.5$ the wake behind the rods merges to form clusters and moves in a synchronized inphase pattern. Awale [17] observed that the inner two circular rods experience high drag compared to outer two rods in his study of flow past row of circular rods using ANSYS software. He investigated synchronized flow at $g \geqslant 6$, Quasi-Periodic-I flow at $3 \leqslant g \leqslant 5$, Quasi-Periodic-II flow at $g = 2$ and chaotic flow at $g \leqslant 1$. Mizushima and Akinaga [18] experimentally and numerically investigated the interactions of flow past a row of square and circular bars. They identified the inphase vortex shedding at $g = 1$ and antiphase vortex shedding at $g = 3$. In the aforesaid studies mostly emphasis was given on flow patterns but in some studies the time-trace analysis of drag and lift coefficients and spectrum analysis are also given [19,20].

Kumar et al. [19] observed three distinct flow features for nine side-by-side square rods at $g = 0.3$–12 and $Re = 80$ using the lattice Boltzmann method. They observed no significant interaction between the wakes at $g > 6$ and synchronized, quasi-periodic and chaotic flow patterns at relatively smaller gap spacings. Chatterjee et al. [20] performed a numerical study for five side-by-side square rods at $Re = 150$ over $g = 1.2$–4. They identified four flow patterns, each characterized by a distinctive wake structure mechanism behind the rods in terms of vortex shedding, time-trace analysis of drag and lift coefficients and existence of secondary interaction frequencies together with primary vortex shedding frequency due to jet flow between the gaps. They identified antiphase flow pattern at $g = 4$, inphase and antiphase flow pattern at $g = 3$ and flip-flopping wake pattern at $g = 1.2$. Chatterjee et al. [20] only provide the average mean drag coefficient (Cdmean) and Strouhal number value for different gap spacing. For rows of staggered square rods Chatterjee and Biswas [21] observed organized periodic flow for large g but as g decreases the flow changes its state from organized periodic to quasi-periodic, then transitional and finally completely chaotic.

However, there is no detail qualitative and quantitative information available in relation to flow past row of rectangular rods with aspect ratio $R = 0.5$. For example, how the flow will behave for different aspect ratios? What kind of wake structure interactions is associated behind the rods with change in spacings? How do the physical parameters behave with the gap flow switch? How secondary frequencies appear together with the primary vortex shedding frequency due to jet flow interaction? The issues raised above motivate this numerical investigation. Various aspects of flow patterns are examined carefully, including wake structure mechanism behind the rods, switching of flow patterns, downstream flow characteristics and sensitivity of physical parameters. The rest of paper contains problem description and numerical details, grid independence study and code validation and results and discussion, organized in Sections 2, 3, 4, and 5, respectively.

2. Problem description and numerical details

The schematic flow configuration, numerical details for flow past five side-by-side rectangular rods for different gap spacings are discussed in this section.

2.1. Problem description

The computational domain is fixed in streamwise direction (x) and varies in transverse direction (y) for different gap spacings (see Table 1). The schematic flow configuration is shown in Fig. 1. Five fixed two-dimensional rectangular rods with height 'h' and width 'w' are exposed to a uniform inflow with velocity U_∞. The rods are placed side-by-side in the channel of height H. The channel length L is fixed at $50h$. An upstream length of Lu = $6h$ and downstream length of Ld = $43.5h$ have been chosen. The five rods are arranged from bottom to top. In Fig. 1, c_1, c_2, c_3, c_4 and c_5 represent first, second, third, fourth and fifth rods, respectively.

Table 1 Selected cases for computations.

Cases	$H \times L$
$g = 1$	381×1001
$g = 1.5$	421×1001
$g = 2$	461×1001
$g = 2.5$	501×1001
$g = 3$	541×1001
$g = 4$	621×1001
$g = 5$	701×1001
$g = 6$	781×1001

2.2. Numerical details

Instead of solving the usual continuum equations for fluid fields, the Lattice Boltzmann method (LBM) models fluid flow by tracking the fluid particles evolution where at each time step the physical space is discretized into a number of square regu-

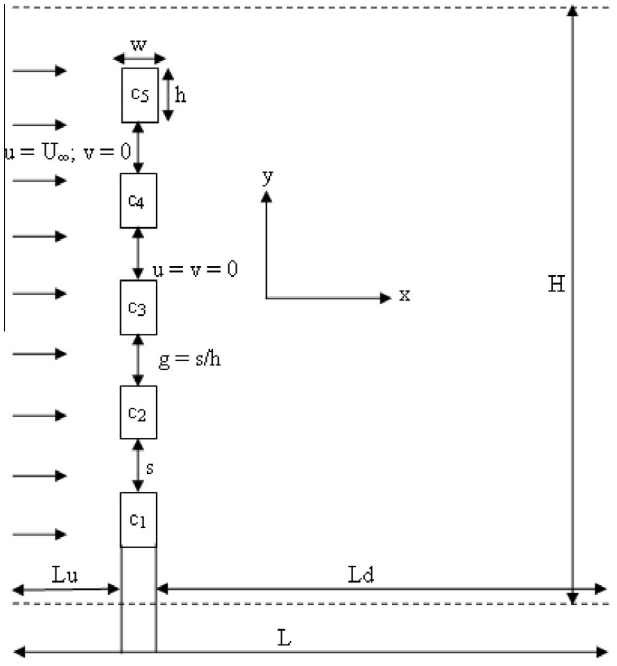

Figure 1 Schematic configuration of flow past five side-by-side rectangular rods.

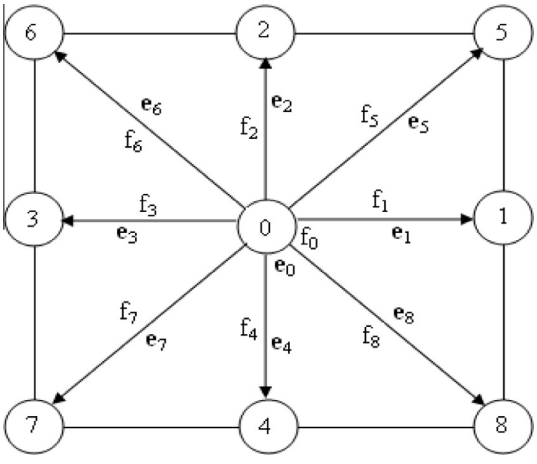

Figure 2 Discrete velocity directions.

lar lattices (Fig. 2). It has two main steps: (i) streaming and (ii) collision. LBM has several advantages over conventional techniques. For example the streaming and collision are local in nature which provides the opportunity of parallel computing [22]. LBM is explicit and can easily handle the nonlinear term in Navier-Stokes equation [23]. Moreover there is no need to solve Laplace equation in each time step for the calculation of pressure as it can be obtained by solving the equation of state [22]. Moreover it is second order accurate in both space and time and can handle complex geometries efficiently [22,23]. Different models can be used in LBM for fluid flows [22]. In this study, a two-dimensional nine-velocity (D2Q9, where D is the space dimensions and Q is the number of particles) model used in standard Boltzmann equation is adopted [22–26].

The evolution density distribution function of the fluid particles can be described by

$$f_i(\mathbf{x}+\mathbf{e}_i, t+1) = f_i(\mathbf{x}, t) - [f_i(\mathbf{x}, t) - f_i^{(eq)}(\mathbf{x}, t)]/\tau \quad (1)$$

where f_i is the particle distribution function at position $\mathbf{x}$ and time t, $f_i^{(eq)}$ is the corresponding equilibrium distribution function, $\mathbf{e}_i$ is the direction of velocity and τ is the relaxation time.

The equilibrium distribution function is computed as below

$$f_i^{(eq)} = \rho w_i[1 + 3(\mathbf{e}_i.\mathbf{u}) + 4.5(\mathbf{e}_i.\mathbf{u})^2 - 1.5\mathbf{u}^2], \quad i = 0, 1, 2, \ldots, 8 \quad (2)$$

where at each computational node $\mathbf{u}$ is the instantaneous velocity and w_i are corresponding weighting functions ($w_i = 4/9$ for $i = 0$, $w_i = 1/9$ for $i = 1, 2, 3, 4$ and $w_i = 1/36$ for $i = 5, 6, 7, 8$). The kinematic viscosity of fluid can be obtained in the following way

$$v = (2\tau - 1)/6\Delta t, \quad (3)$$

where Δt is the lattice time step and is equal to one in this study.

The pressure (p) is determined by the isothermal equation of state

$$p = \rho c_s^2, \quad (4)$$

where c_s is the artificial speed of sound, and is equal to 0.5774 in this model (Wolf-Gladrow [23]). The flow velocity $\mathbf{u}$ and density ρ can be obtained by

$$\rho = \sum f_i \quad \text{and} \quad \rho\mathbf{u} = \sum f_i\mathbf{e}_i, \quad i = 0, 1, 2, 3, \ldots, 8 \quad (5)$$

Uniform flow with velocity U_∞ is incorporated using the equilibrium particle distribution function at the inlet boundary where

$$\boldsymbol{u} = U_\infty \quad \text{and} \quad \boldsymbol{v} = 0. \quad (6)$$

The computational domain behind the rods is selected to be large enough so that the flow at outlet boundary can be considered to be fully developed. Therefore a fixed pressure in terms of the equilibrium distribution function is imposed at the outlet. For such implementation, the velocity components are extrapolated at downstream (Cheng et al. [25]). A no-slip ($\boldsymbol{u} = \boldsymbol{v} = 0$) wall boundary condition is applied on the surfaces of rod (Ziegler [26]). Periodic boundary condition [27] is applied at both bottom and top boundaries of the computational domain. The total fluid forces on rectangular rods are calculated using the momentum exchange method [28].

Some important physical parameters are used in this paper which are defined as follows

The Reynolds number is defined as

$$Re = U_\infty h/v \quad (7)$$

where h is the size of the rod and v is the kinematic viscosity.

The Strouhal number, drag coefficient, lift coefficient and root-mean-square value of drag and lift coefficients (Cdrms and Clrms) are given as

$$St = f_s h/U_\infty \quad (8)$$

$$\mathrm{Cd} = \mathrm{Fd}/0.5\rho U_\infty^2 h \quad (9)$$

$$\mathrm{Cl} = \mathrm{Fl}/0.5\rho U_\infty^2 h \quad (10)$$

$$\mathrm{Cdrms} = \sqrt{\sum_{t=1}^{n}[\mathrm{Cd}(t) - \overline{\mathrm{Cd}}(t)]^2/n} \quad (11)$$

$$\mathrm{Clrms} = \sqrt{\sum_{t=1}^{n}[\mathrm{Cl}(t) - \overline{\mathrm{Cl}}(t)]^2/n} \quad (12)$$

where f_s is the vortex shedding frequency, Fd and Fl are the force components in in-line and transverse directions, respectively, $\overline{\mathrm{Cd}}$ and $\overline{\mathrm{Cl}}$ are the mean of drag and lift coefficients, respectively and n is the total number of time steps. All the computations are carried out on a Dawning Parallel Computer TC4000.

3. Grid independence study and code validation

3.1. Grid independence study

A grid independence study is carried out for different combinations of Lu, Ld and H for flow past five side-by-side rectangular rods at $g = 5$. The computational results of average mean drag coefficients, Strouhal number, root-mean-square values of drag and lift coefficients for five rods obtained for different cases are summarized in Table 2, and the discrepancies between the results for different combinations in percentage are also given. We have selected Lu = 6h, Ld = 43.5h and H = 11h (excluding the rods and gap spacings) for all numer-

Table 2 Grid independence study at $g = 5$.

Cases	Cdmean	St	Cdrms	Clrms
Lu = 6h; Ld = 43.5h; H = 35h	2.1183 (0.52%)	0.1905 (0%)	0.0520 (0.77%)	0.1091 (0.18%)
Lu = 8h; Ld = 43.5h; H = 35h	2.1072	0.1905	0.0516	0.1093
Lu = 6h; Ld = 43.5h; H = 35h	2.1183 (0.75%)	0.1905 (0.16%)	0.0520 (0.38%)	0.1091 (0.18%)
Lu = 6h; Ld = 35h; H = 35h	2.1342 (0.76%)	0.1902 (0.16%)	0.0522 (0.57%)	0.1089 (0.09%)
Lu = 6h; Ld = 50h; H = 35h	2.1181	0.1905	0.0519	0.1090
Lu = 6h; Ld = 43.5h; H = 33h	2.1172 (0.05%)	0.1906 (0.05%)	0.0518 (0.38%)	0.1092 (0.09%)
Lu = 6h; Ld = 43.5h; H = 35h	2.1183 (0.06%)	0.1905 (0.05%)	0.0520 (0.38%)	0.1091 (0.18%)
Lu = 6h; Ld = 43.5h; H = 37h	2.1170	0.1906	0.0518	0.0193

ical results in this study and compared with other combinations. It can be noted that in case of $g = 5$, the value of $H = 35h$ included the rods and gap spacings in Table 2. One can also use Ld = $35h$ and $H = 33h$ for such flow configurations. The reason is that we give enough domain space to shed vortices behind the rods and also from the top corner of c_5 and bottom corner of c_1 of the rods, and have not observed more than one percent difference between physical parameters in any combination. In other combinations such as Ld = $50h$ and H = $37h$, more grid points are needed without any significant affect on flow and physical parameters.

3.2. Code validation

The numerical code is validated against the problem of flow past a single square rod for $Re = 100$, 150 and 200. It is noted that we chose square rod instead of rectangular rod with aspect ratio $R = 0.5$, because enough experimental and numerical data were available for comparison and not too much data available for $R = 0.5$, except one experimental [5] at high Reynolds number and one numerical [7]. Two important parameters are validated: mean drag coefficient and Strouhal number. The experimental data of Okajima [1] and Sohankar et al. [2] as well as numerical results of Gera et al. [3], Chatterjee et al. [20] and Cheng et al. [25] are given in Table 3 for comparison. It is observed that the present calculations of Cdmean at $Re = 150$ are in good agreement with the experimental data of Okajima [1] and very close to the numerical data of Gera et al. [3]. The Strouhal numbers obtained in the present work have shown a good agreement with the experimental data of Sohankar et al. [2] and numerical data of Chatterjee et al. [20] at $Re = 150$. The general trend is almost similar to that observed by Okajima [1] experimentally and numerically by Gera et al. [3], Chatterjee et al. [20] and Cheng et al. [25].

4. Results and discussion

In this section, the effect of the gap spacing on hydrodynamic parameters such as flow patterns, time series for force coefficients, power spectra analysis of lift coefficients and vorticity contours visualization for different flow patterns is discussed. Calculations of the statistics, mean drag coefficients, Strouhal number, root-mean-square values of drag and lift coefficients, average mean drag coefficient and Strouhal number for five rods are also given. It is important to mention here that we calculate Strouhal number using the Fast Fourier Transform (FFT) technique. In vorticity graphs the solid lines represent positive vortices generated from the lower corner and dashed line represents negative vortices generated from the upper corner of rods. In this study we have used Cdmean1, Cdmean2, Cdmean3, Cdmean4, Cdmean5, for mean drag coefficients, St1, St2, St3, St4, St5, for Strouhal numbers, Cdrms1, Cdrms2, Cdrms3, Cdrms4, Cdrms5, for root-mean-square value of drag coefficients and Clrms1, Clrms2, Clrms3, Clrms4, Clrms5, for root-mean-square value of lift coefficients, for first, second, third, fourth and fifth rods, respectively. In drag and lift coefficient graphs we have used bold solid, bold dashed, bold dotted, bold dash-dotted and normal lines for first, second, third, fourth and fifth rods, respectively. It is also important to state here that repeated results are not mentioned here, due to similar characteristics. We assign name to flow patterns on the basis of previous studies exist in the literature and the characteristics of flow and time-trace analysis of drag and lift coefficients observed in this investigation. In spectra graphs 'E' represents the spectrum energy.

Table 3 Comparison of present and previous experimental and numerical results.

	$Re = 100$		$Re = 150$		$Re = 200$	
	Cdmean	St	Cdmean	St	Cdmean	St
Present	1.41	0.146	1.42	0.154	1.48	0.155
Okajima [1]	...	0.139	1.45	0.141	1.42	0.144
Sohankar et al. [2]	...	0.143	...	0.155	...	...
Gera et al. [3]	1.46	0.129	1.41	0.141	1.49	0.143
Chatterjee et al. [20]	...	0.141	...	0.156	...	...
Cheng et al. [25]	1.44	0.144	...	...	1.45	0.152

4.1. Flow patterns

The vorticity contour visualization and its corresponding drag and lift coefficients at $g = 1$ are shown in Fig. 3(a)–(c). At this small gap spacing the jets between the rectangular rods are totally deviated and as a result complex flow pattern is observed behind the rods. Such kinds of flow feature are generally observed in the wind-tunnel grids. The corresponding spectra of lift coefficients are given in Fig. 4(a)–(e). The vortex formations near downstream of rods are not quite clear and have great influence on flow structure at further downstream (Fig. 3(a)). This flow pattern is named as flip-flopping. The time-trace analysis of drag coefficients shows how the flow in the flip-flopping pattern modifies with time and has more chaotic behavior as compared to time-trace analysis of lift coefficients (Fig. 3(b) and (c)). This reveals that the merging and distortion of vortices actually happen due to decoupling of drag and lift coefficient dynamic.

In this complex flow pattern the rods would experience fluctuating forces with higher frequency at downstream of the computational domain. Therefore, the power spectra analysis of lift coefficients shows a strong interaction of multiple frequencies together with the primary vortex shedding frequency (Fig. 4(a)–(e)). This is due to the jet interaction with the shed vortices behind the rods and as a result one can see the vortex shedding frequency together with jet-induced frequency. In spectrum analysis we select highest peak as a primary vortex shedding frequency. Kumar et al. [19] and Chatterjee et al. [20] have observed such flow characteristics for nine and five side-by-side square rods, respectively. It is clear from Fig. 4 (a)–(e) that the overall spectrum of first and fifth and second and fourth rods shows similar behavior. Due to this result, in the rest of paper only the spectrum of first three rods or the spectrum of last three rods is shown.

Fig. 5(a)–(c) shows the vorticity contour visualization and drag and lift coefficients against time at $g = 1.5$. The corresponding spectra are given in Fig. 6(a)–(c). The narrow gap spacing between the rods prevents the shed vortices to fully

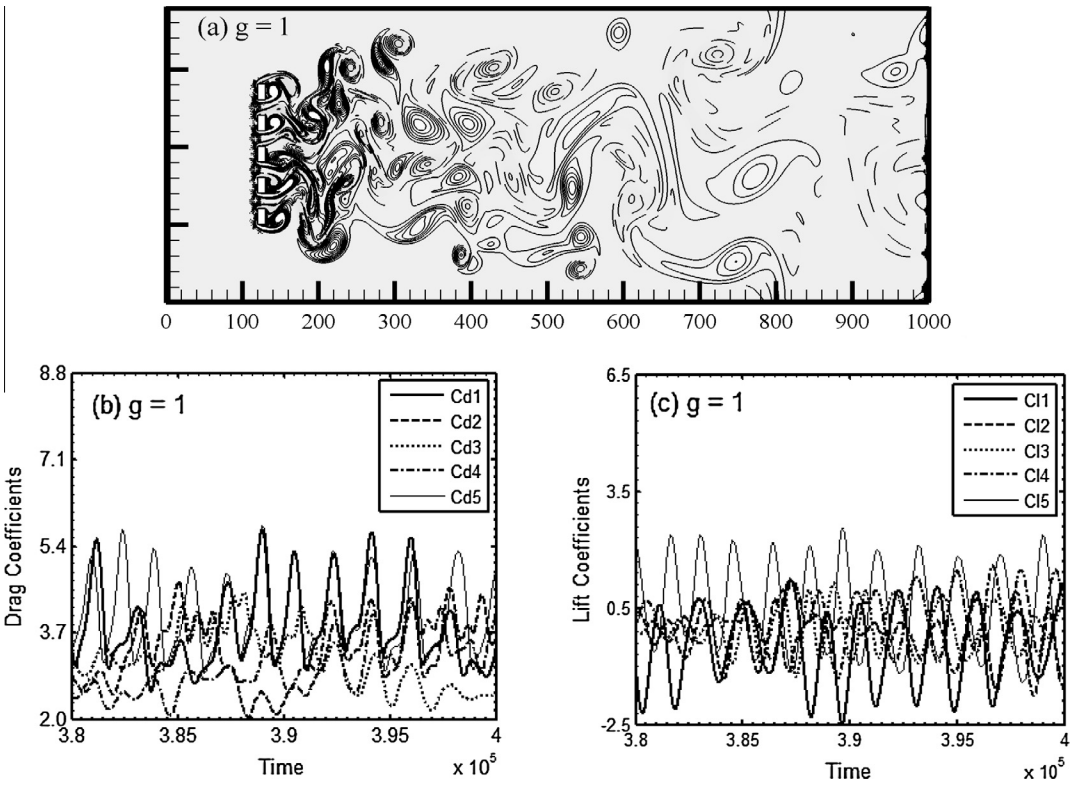

Figure 3 (a–c) Vorticity contour visualization, time-trace analysis of drag and lift coefficients for flip-flopping flow pattern.

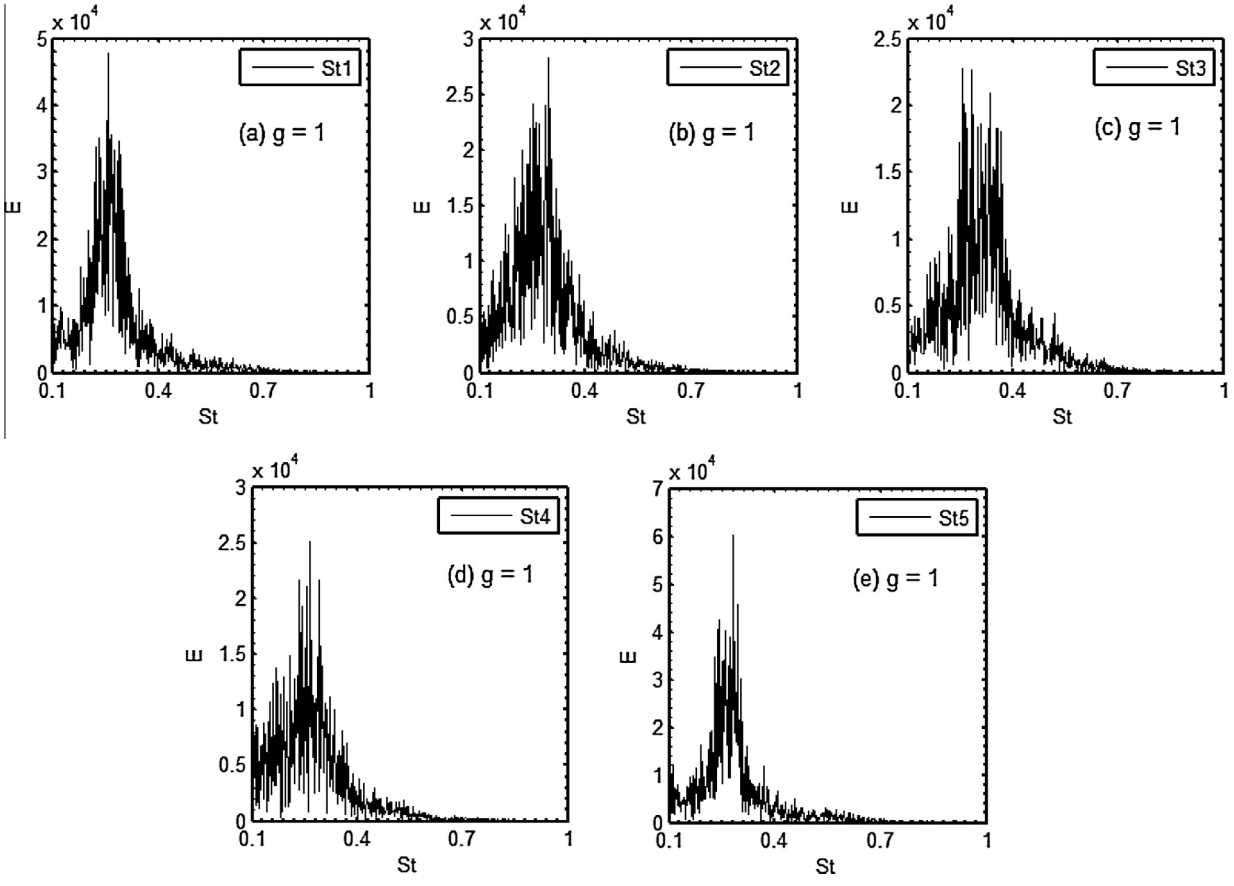

Figure 4 (a–e) Power spectra analysis of lift coefficients for flip-flopping flow pattern.

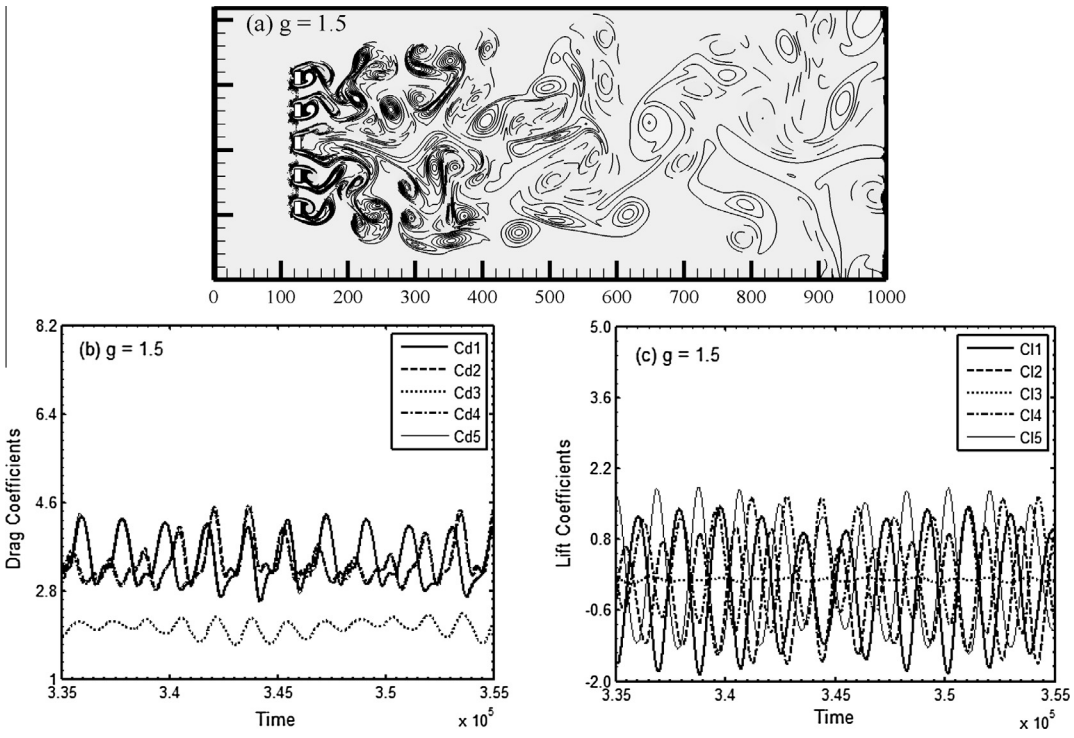

Figure 5 (a–c) Vorticity contour and time-history plots for $g = 1.5$.

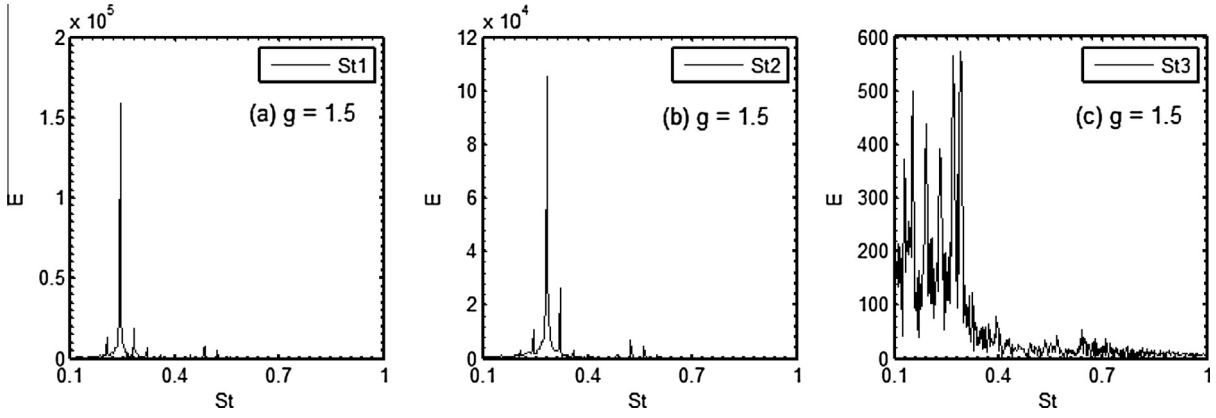

Figure 6 (a–c) Power spectra analysis of lift coefficients plots for $g = 1.5$.

develop. At this small g, in the observed flip-flopping pattern we notice several differences from those at $g = 1$. Firstly, the wake of the third rod is nearly unsteady and affects the wake structure far downstream of the computational domain. Secondly, the antiphase behavior is observed for the first and second rods and for fourth and fifth rods. Therefore, the gap flows between the second and third as well as third and fourth rods are observed to be weaker (Fig. 5(a)). This leads to a decrease in fluctuating drag and lift coefficients (Fig. 5 (b) and (c)) acting on rods as compared to $g = 1$ (Fig. 3(b) and (c)) case.

From power spectrum graphs, some small peaks can be observed due to weak jet-induced frequency between the gaps compared to $g = 1$ case are observed. Beside the amplitude of the drag and lift coefficients compared to $g = 1$, the spectra of the lift coefficients also change, which is a clear indication that the shedding frequency behind the rectangular rods is changed. The oscillation exhibits a dominant vortex shedding frequency together with some small peaks except the third rod which behaves nearly unsteady and at far downstream the shed vortices from the second and fourth rods merge with the nearly unsteady vortices generated from the third rod.

Fig. 7(a)–(c) shows the flow structure and time-trace analysis of drag and lift coefficients for the nearly unsteady-inphase flow pattern case. Furthermore, Fig. 8(a)–(d) shows the spectrum analysis of the lift coefficients for this flow pattern. Kumar et al. [19] and Chatterjee et al. [20] have not observed this kind of flow pattern for flow past nine and five side-by-side square rods. The general flow features and its effect on the time-trace analysis of drag and lift coefficients and power spectra analysis of lift coefficients are noticeable. The first major change is that the third rod behaves nearly unsteady.

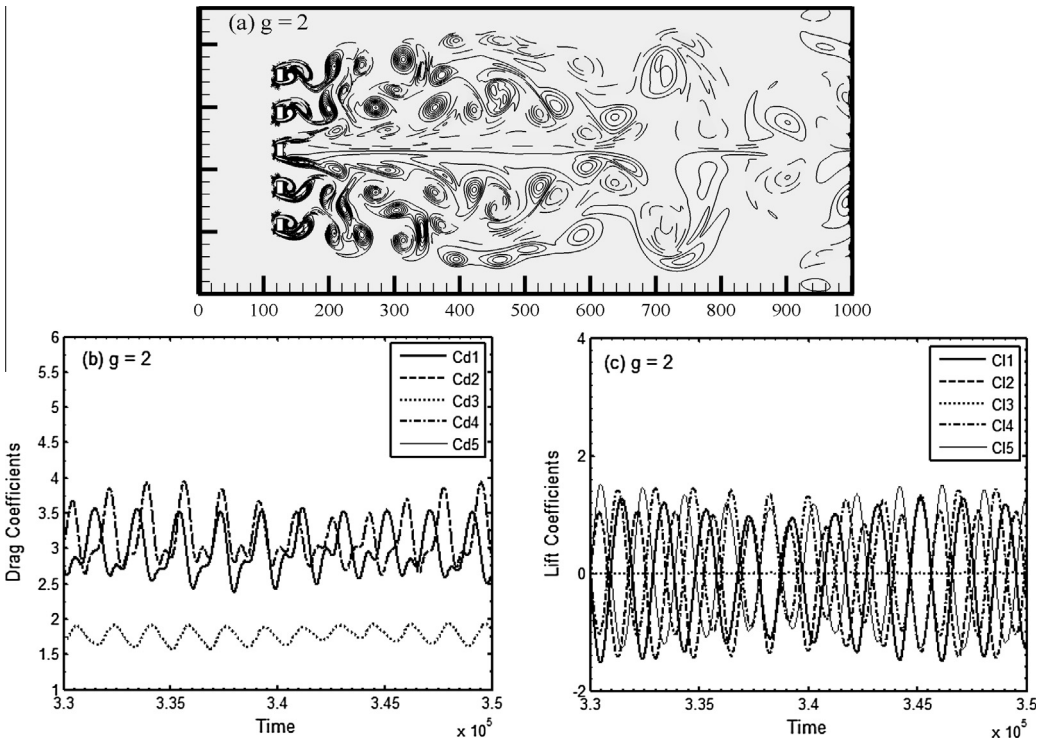

Figure 7 (a–c) Vorticity contour and time signal analysis plots for $g = 2$.

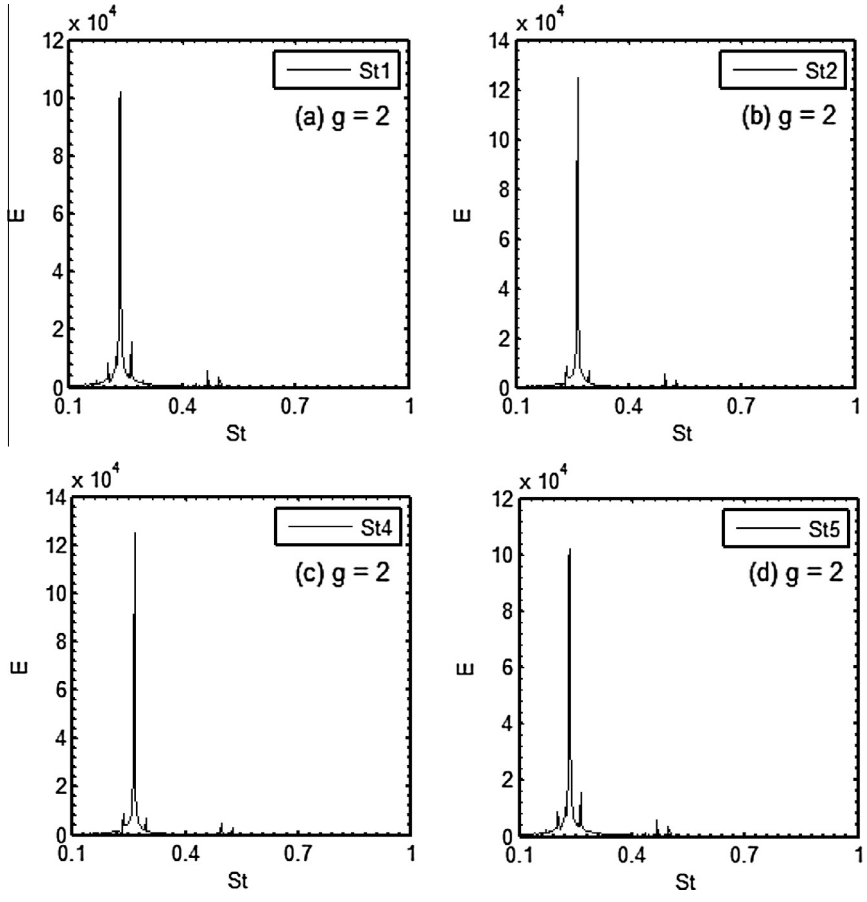

Figure 8 (a–d) Spectra lift coefficients analysis plots for $g = 2$.

Initially, the negative and positive vortices are just appeared and then become weaker and weaker further downstream and are not showing any strong interaction with the vortices shed from the second and fourth rods (Fig. 7(a)). The inphase flow structure is observed for first and second as well as for the fourth and fifth rods. This flow structure is called the nearly unsteady-inphase flow pattern. Moreover, it is noted the lift coefficients of c_1-c_2, c_1-c_4 and c_4-c_5 either inphase or antiphase with time variation, but the inphase variation is dominant (Fig. 7(c)).

For this flow pattern, we have not calculated the Strouhal number of the third rod because of nearly constant behavior of lift fluctuation. As the gap spacing is further increased to 2, the existences of some secondary rod interaction frequencies are notable but not dominant and as a result modulation is observed in the lift coefficient signals. This modulation arises from the interactions of primary and secondary rod interaction frequencies due to jet flows between the rods. The same shedding frequencies are observed for the first and fifth as well as for the second and fourth rods (Fig. 8(a)–(d)).

Fig. 9(a)–(c) shows the time-trace analysis of the drag and lift coefficients together with the vorticity contour visualization at $g = 2.5$. The inphase and antiphase alternate variation of vortex shedding from c_1–c_2, c_1–c_3, c_1–c_4 and c_1–c_5 can be seen. For other combinations such as c_2–c_3, c_2–c_4, c_2–c_5, c_3–c_4, c_3–c_5 and c_4–c_5 either antiphase or inphase vortex shedding is observed. One can see the merging of vortices '7*h*' downstream of the rods and more complex flow structure and distortion of vortices observed at far downstream location. The comparison of vortex shedding between rods shows definite phase relationship. The inphase vortex shedding is dominant. Alam and Zhou [10] experimentally observed that gap flow for two side-by-side square rods at $Re = 4.7 \times 10^4$ and $2.1 \leqslant g \leqslant 2.4$ biased downward, upward or unbiased, and as a result antiphase vortex shedding and inphase vortex shedding are observed for different combinations. It is important to mention here that the variations of lift coefficients are close to 0° and 180° for inphase and antiphase vortex shedding. In case of $g = 2.5$, the vortex shedding only closes to inphase or antiphase. Chatterjee et al. [20] also examined the close inphase or antiphase vortex shedding for flow past five side-by-side square rods.

The above observations related to inphase and antiphase synchronized shedding can also be clarified by viewing the time-trace analysis of lift coefficients of two consecutive rods (see Fig. 11(a)–(d)). Moreover, the lift coefficients are sinusoidal in nature and the modulated behavior observed for drag coefficients (Fig. 9(b) and (c)). This is due to the jet interactions created by the gap spacings and as a result the shed vortices no longer remain distinct throughout the computational domain. The observation implies that the vortices are not yet stable throughout the computational domain, probably because of strong interactions between vortices far downstream of computational domain. On the basis of such characteristics the flow pattern is named as modulated inphase-antiphase synchronized flow pattern. The comparison of power spectrum analysis of three rods is shown in Fig. 10 (a)–(c). Due to merging of flow at far downstream one can see some secondary rod interaction frequencies for the second and fourth rods (Fig. 10(b)). The same flow features and time signal characteristics are observed for the case $g = 3$ and also found the merging of vortices at far downstream locations (not shown).

Fig. 12(a)–(c) shows the wake structure and time signal analysis of drag and lift coefficients for $Re = 150$ and $g = 6$.

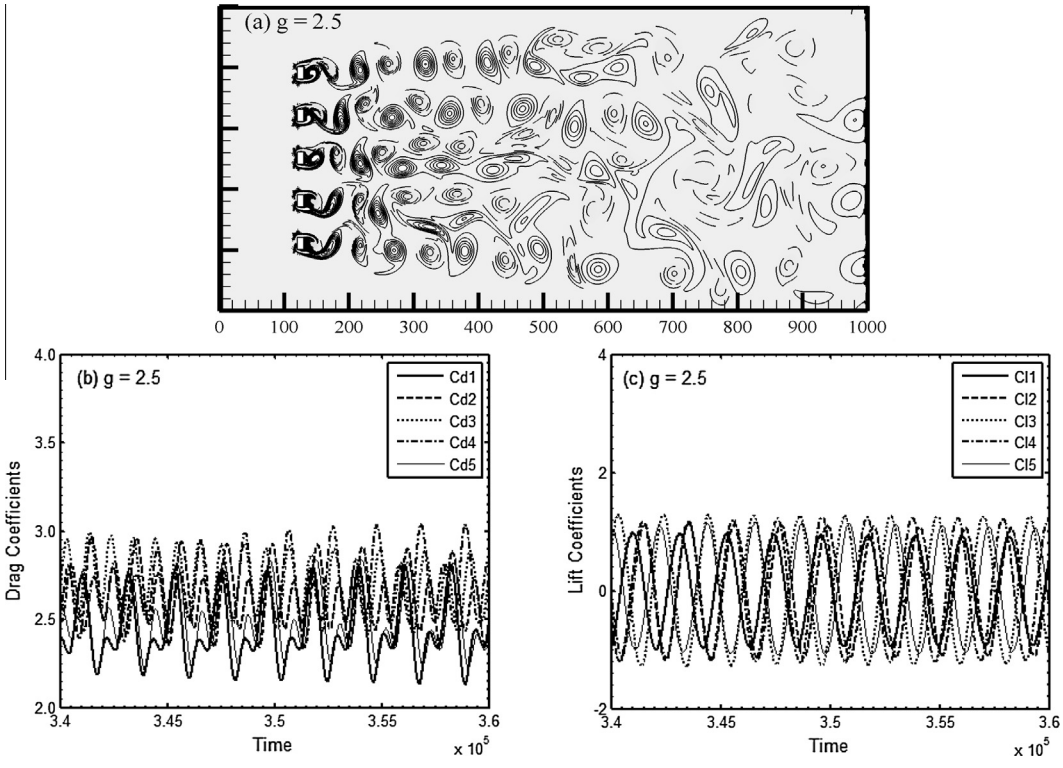

Figure 9 (a–c) Vorticity contour and signal analysis for in-phase flow pattern.

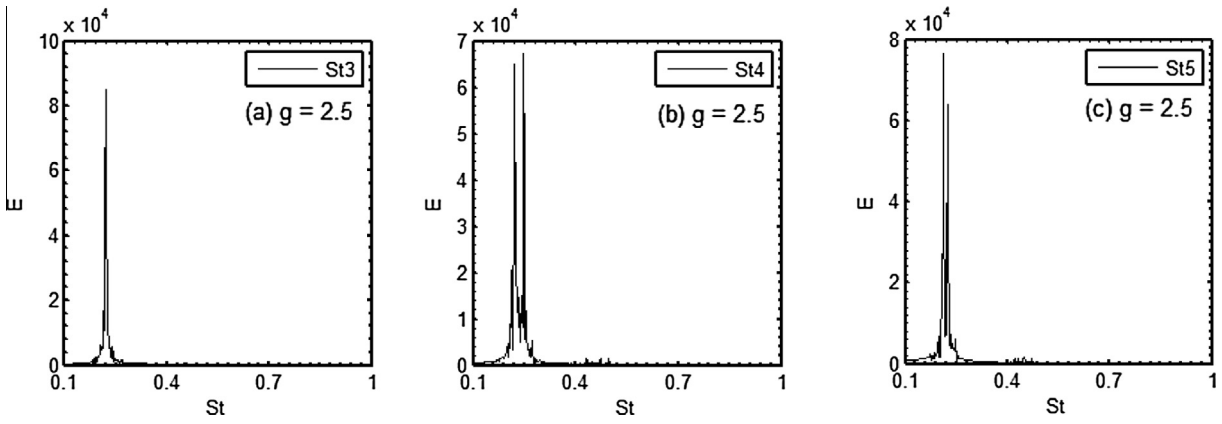

Figure 10 (a–c) Spectrum analysis for inphase-antiphase synchronized flow pattern.

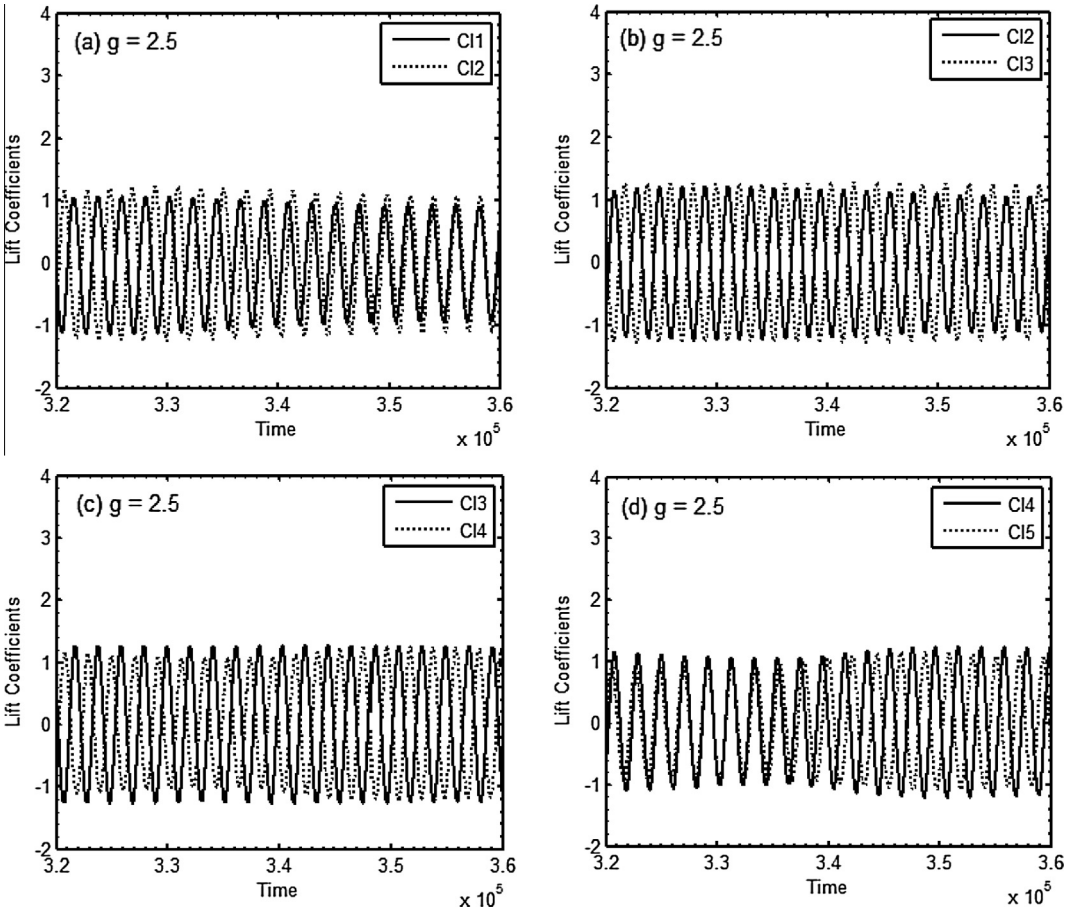

Figure 11 (a–d) Time-trace analysis of lift coefficients.

We check the successive combinations of rods for vortex shedding behind the rods. It is observed that the vortex shedding behind c_1 and c_2 is inphase. The other combinations c_1–c_3, c_1–c_4, c_1–c_5, c_2–c_3, c_2–c_4, c_2–c_5, c_3–c_4, c_3–c_5 and c_4–c_5 are inphase, inphase, antiphase, inphase, inphase, antiphase, antiphase, inphase, and inphase, respectively. The vortices behind the rods do not show merging and distortion behavior throughout the computational domain. This is a kind of weakly interactive flow pattern arising at large gap spacing between the rods. This result evidences that inphase vortex shedding is predominant as compared to antiphase vortex shedding for successive combination of rods. It is important to mention here that Chatterjee et al. [20] observed that antiphase vortex shedding is predominant at large gap spacing between the square rods, whereas we observe that the inphase vortex shedding is predominant for aspect ratio $R = 0.5$. This may be due to smaller vortex formation region for rectangular rods with aspect ratio less than one. Abdollah et al. [5] exper-

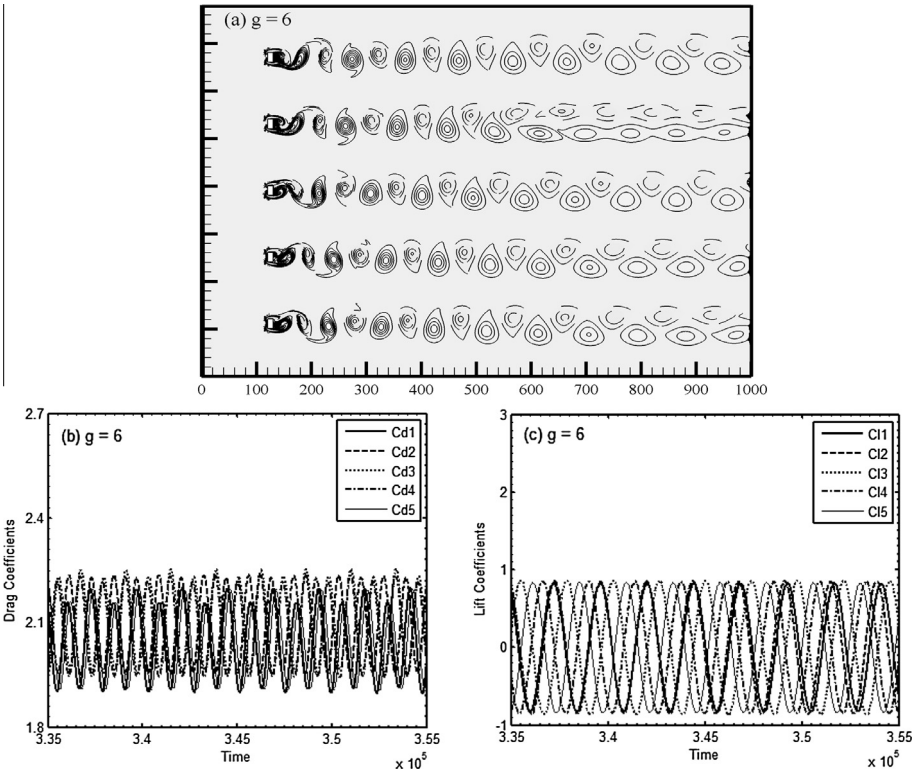

Figure 12 (a–c) Flow and drag and lift coefficient analysis for synchronized flow pattern.

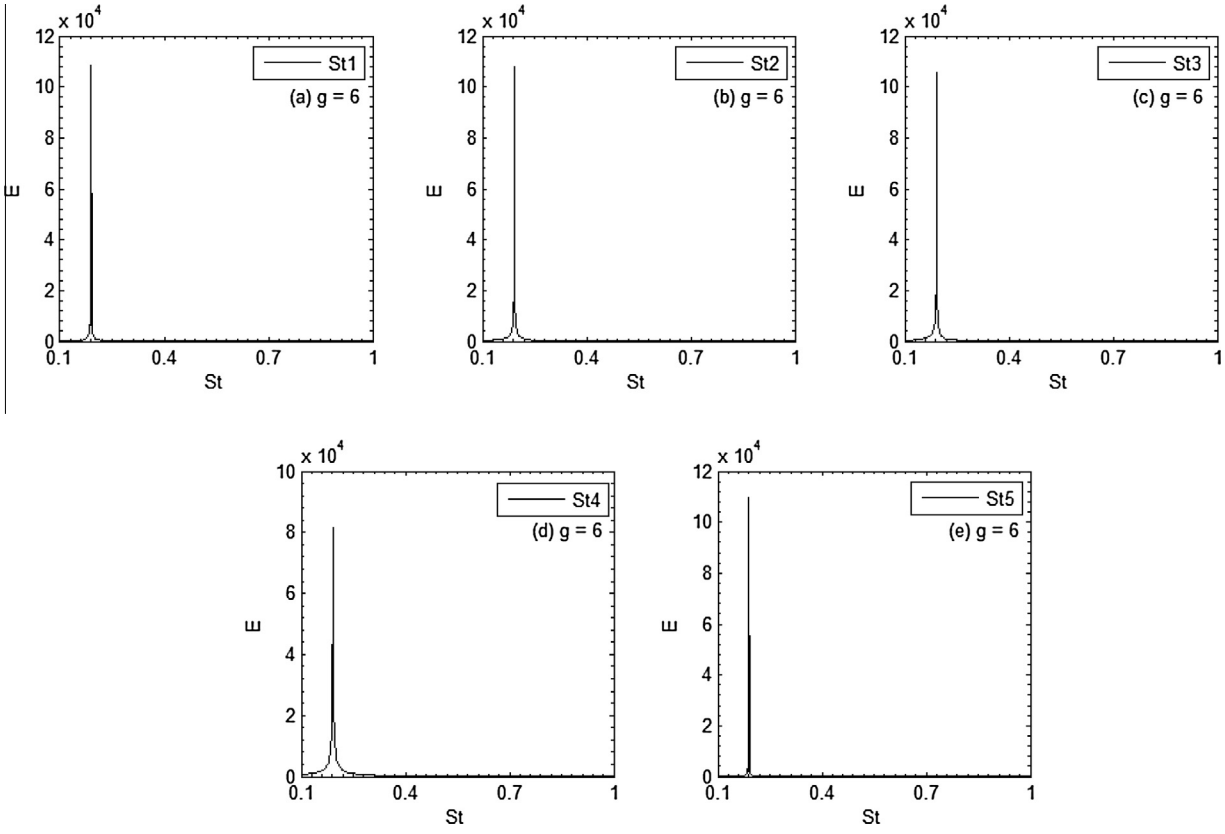

Figure 13 (a–e) Lift coefficients spectrum analysis for synchronized flow pattern.

imentally and Islam et al. [7] numerically already observed such kind of vortex formation for flow past single rectangular rod. Alam and Zhou [10] experimentally proposed that if the convection velocity is same for all vortices then the shed vortices between consecutive rods are either antiphase or inphase for two side-by-side square rods.

The above synchronized vortex shedding observations regarding the inphase and antiphase can also be justified by looking into the time-trace analysis of drag and lift coefficients (Fig. 12(b) and (c)) of five rods and two consecutive rod combinations (Figs. 14 and 15(a)–(d)). The results show that the drag and lift coefficients are sinusoidal in nature. The sinusoidal nature of lift coefficient reveals that all the rods behave like a single rod. One can also see that in some combinations the shedding is not perfectly inphase or antiphase, only close to them. The present results also reveal that the oscillation time period of drag coefficient is about half of the oscillation time period of lift coefficient for any two consecutive rods combination.

Fig. 13(a)–(e) represents the spectrum analysis of lift coefficients, for all five rods (representative cases). The vortex shedding frequency for such flow pattern can be determined from the power spectra analysis of lift coefficients for each rod. It is observed that only primary vortex shedding frequency is predominant and there is no evidence of secondary rod interaction frequencies due to sinusoidal nature of lift fluctuations. This reveals that the jet flow effect between the gaps diminishes at large gap spacing. The amplitude of the fourth rod is less than other rods and as a result one can see the two row-vortex street behavior near the exit of the computational domain behind the fourth rod. The jet flow effect between the gaps is almost negligible even for $g = 4$. The stability of the shed vortices is enhanced at large gap spacings. Another notable feature of the shed vortices is that the antiphase shed vortices are dominant than the inphase. The similar vorticity contour visualization, time-trace analysis of drag and lift coefficients and power spectra analysis of lift coefficients are observed for $g = 4$ and 5 (not shown) in this study.

4.2. Data analysis

The results of the mean drag coefficient, Strouhal number, root-mean-square values of drag and lift coefficients together with the single rectangular rod data (dotted bold line) for comparison are shown in Fig. 16(a)–(d). At $g = 1$, the mean drag coefficient of the third rod is much higher than those for the second and fourth rods in the flip-flopping flow pattern. Moreover, the Cdmean of third rod drops and attains its minimum value at $g = 2$ compared to those of other four rods (Fig. 16 (a)). Guillaume and LaRue [15] experimentally claimed in case of three side-by-side circular rods that the Cdmean value for the middle rod dropped below the values for the other two

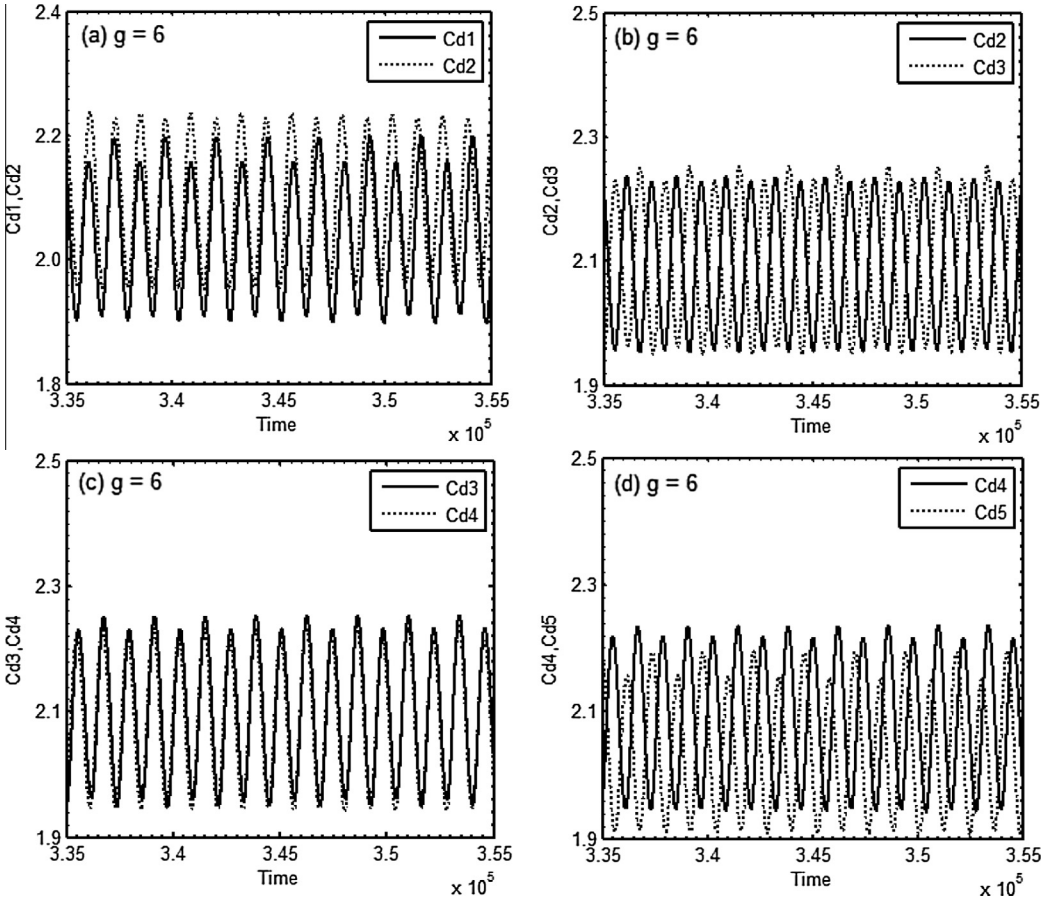

Figure 14 (a–d) Time-history analysis of drag coefficients for $g = 6$.

outer rods in turbulent regime when the symmetric-biased mode occurred. Awale [17] also observed that the inner two circular rods experience high drag compared to outer two rods for flow past row of four circular rods. We observed this important result in case of five side-by-side rectangular rods at low Reynolds number ($Re = 150$). The results further show that in inphase-antiphase modulated synchronized flow patterns the mean drag coefficients of the first and fifth are the same and similar behavior is observed for second and fourth rods. The mean drag coefficient values of the first and fifth rods decrease as g increases. The Cdmean values of second and fourth rods increase from $g = 1$–1.5 where the flip-flopping flow pattern was observed. Also the Cdmean shows decreasing behavior for other flow patterns dominated by either inphase or antiphase vortex shedding (Fig. 16(a)). The Cdmean3 either decreased or increased for different flow patterns as g increases.

It can be seen that the Strouhal number value of first, second and fifth rods decreases as g increases. The value of the third and fourth rods first shows an increasing behavior from $g = 1$–2 and then decreases as g increases. The results further show that first and fifth rods have same values for larger gap spacings (Fig. 16(b)). Similar characteristics are observed for second and fourth rods. It is important to mention here that we have not calculated the Strouhal value of third rod at $g = 2$. At $g = 2$, the third rod lift coefficient is almost constant. The third rod attains its maximum value at $g = 1.5$, and affected too much when the flow pattern changes. It has been observed that all five rods shed their vortices with frequencies close to the single rectangular rod data ($St = 0.181$). There is a minute difference between the vortex shedding frequencies for all rods from $g = 4$–6. Kang [12] numerically observed such differences in shedding frequencies for three side-by-side circular rods at large gap spacings at $Re = 100$.

It is interesting to mention here that the values of Cdrms1, Cdrms2, Cdrms4 and Cdrms5 decrease with increasing g. The Cdrms3 value shows variation for different g attains its maximum and minimum values and then almost constant for $g = 5$ and 6 (Fig. 16(c)). Moreover, the Clrms3 attains its minimum value at $g = 2$ and much lower than single rod value for flip-flopping flow patterns relatively higher than the single rod value for the modulated synchronized flow pattern (Fig. 16(d)). It is interesting to note that in case of three side-by-side circular rods Kang [12] observed that the two outer rods root-mean-square value of lift coefficients are relatively smaller than the single rod value. This means that the rectangular rod with aspect ratio $R = 0.5$ and circular rod causes differences in terms of physical parameters for different gap spacing. The Clrms3 value is lower than other rods value.

The average mean drag coefficient and Strouhal number in this study are computed from the time average signals of drag and lift coefficients, respectively. In addition, Cdmean(average) and St(average) can be expressed as a function of gap spacing (g).

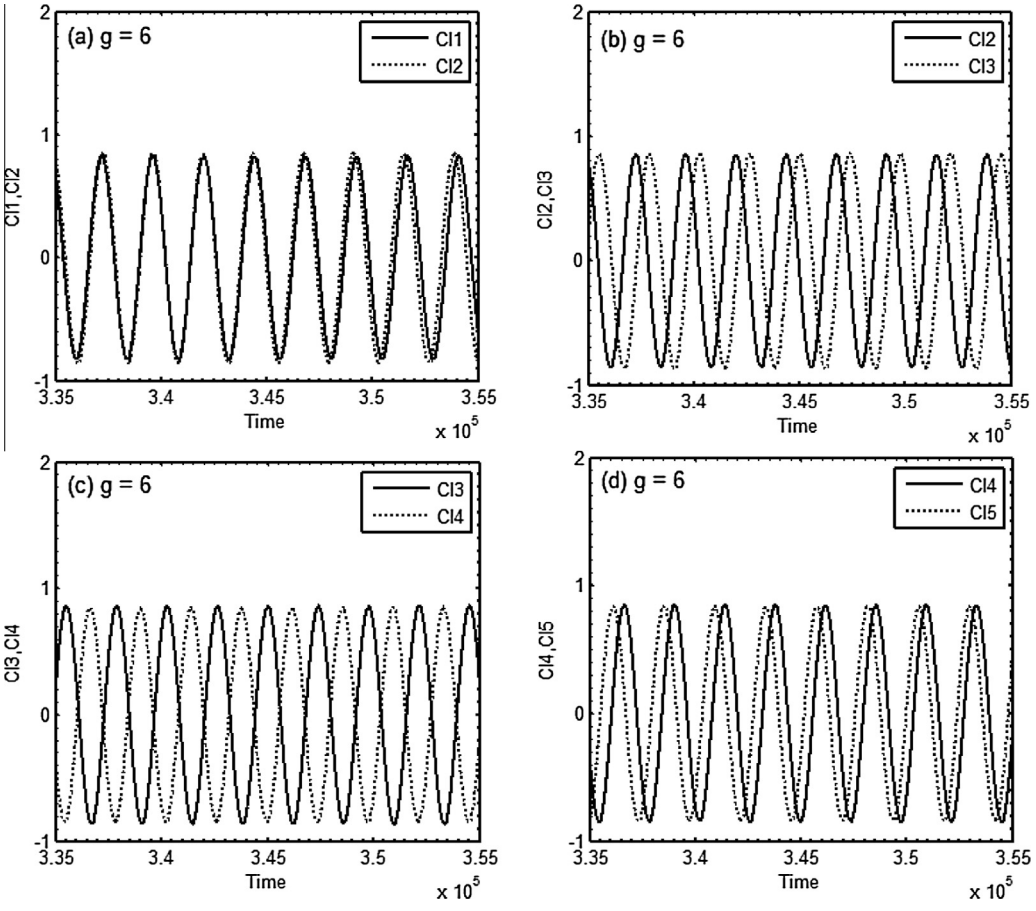

Figure 15 (a–d) Time-trace analysis of lift coefficients for $g = 6$.

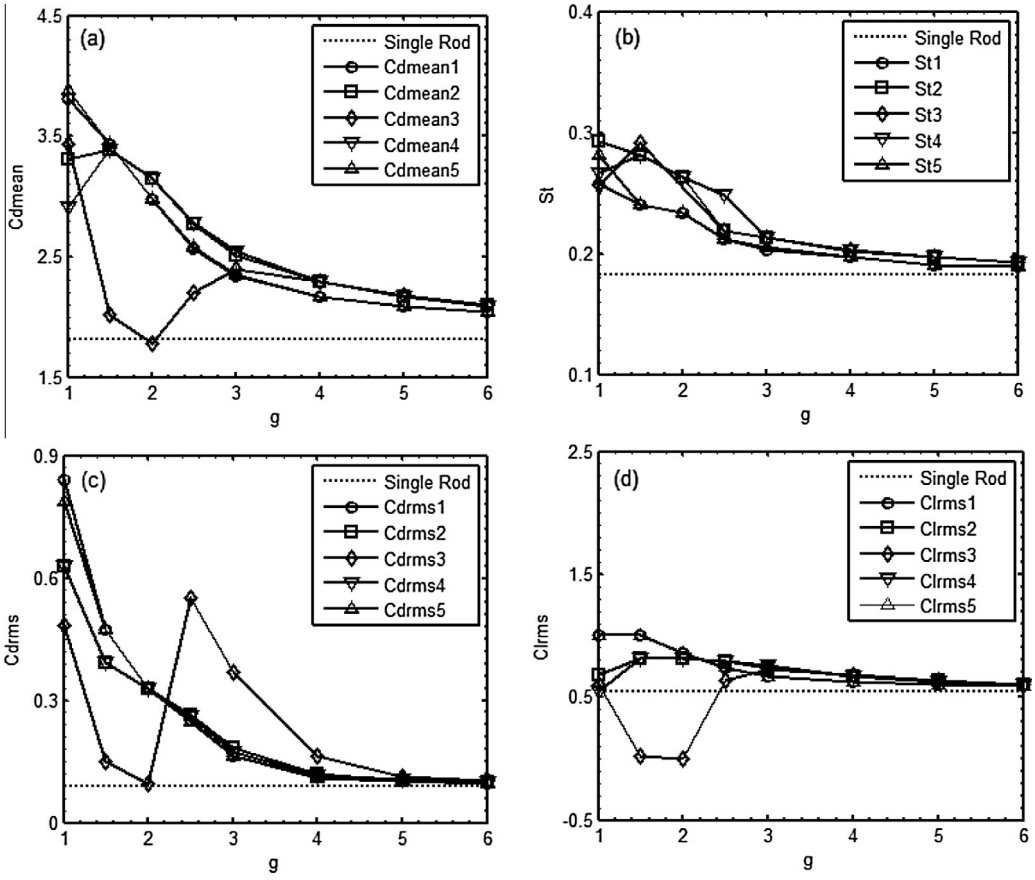

Figure 16 (a–d) Variation of physical parameters versus different gap spacings.

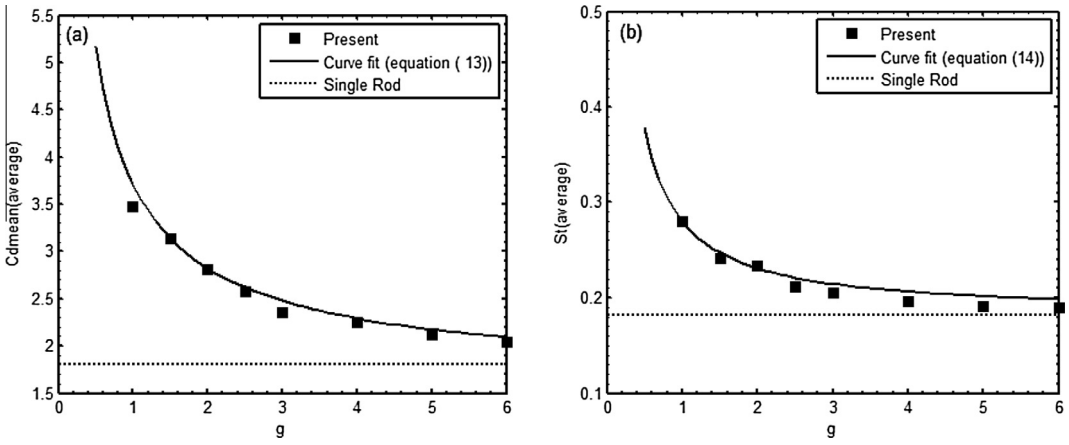

Figure 17 (a and b) Variation of average (a) mean-drag-coefficient and (b) Strouhal number with gap spacing.

$$\text{Cdmean(average)} = 1.81 - 1.3\xi + 3.2\xi^2, \quad \text{where } \xi = g^{-0.32}, \tag{13}$$

$$\text{St(average)} = 0.182 + 0.0982g^{-1}, \quad \text{where } g = (s/h) \tag{14}$$

The aforesaid equations give the values of mean drag coefficient (1.81) and Strouhal number (0.182) for a single rectangular rod ($R = 0.5$) when $g \to \infty$. The variation of average mean drag coefficient and Strouhal number with the gap spacing is depicted in Fig. 17(a) and (b) together with Eqs. (13) and (14). The average mean drag coefficient is found to decrease with increase in the gap spacing which is in good agreement with Eq. (13) (Fig. 17(a)). Similar trend was observed for average Strouhal number (Fig. 17(b)). Chatterjee et al. [20] observed similar characteristics for flow past five side-by-side square rods using different empirical relation. It is also observed that as the value of gap spacing increases the average mean drag coefficient and Strouhal values almost approach to single rectangular rod values.

5. Conclusions

In this study, the flow patterns and force statistics of five side-by-side rectangular rods are investigated using the lattice Boltzmann method. The aspect ratio is 0.5, the Reynolds number is 150 and g ranges from 1 to 6 for present study. The detailed analysis of flow pattern, time-trace analysis of drag and lift coefficients, power spectra of lift coefficients and the presence of secondary rod interaction frequencies are carried out. Important findings are summarized as follows:

(i) There exist four flow patterns for flow past row of rectangular rods: flipflopping at $g = 1$ and 1.5, nearly unsteady-inphase at $g = 2$, modulated inphase-antiphase non-synchronized at $g = 2.5$ and 3 and modulated inphase-antiphase synchronized at $g = 4$–6.

(ii) For different flow parameters, variation in physical parameters is observed. In flip-flopping flow pattern the Cdmean3 is much higher than Cdmean2 and Cdmean4 for $g = 1$. In nearly unsteady-inphase flow pattern, the Cdmean3 drops and attains its minimum value compared to those for four other rods. For other two patterns the Cdmean1 & Cdmean5 and Cdmean2 & Cdmean4 are same. It is also found that $St1$, $St2$ and $St3$ show decreasing behavior for increasing g while $St3$ and $St4$ show variations. The Clrms3 attains its minimum value at $g = 2$ and is much lower than value of single rectangular rod for flip-flopping flow pattern and relatively higher than the single rod value for the modulated inphase-antiphase non-synchronized flow pattern.

(iii) We also have given the empirical relations for average mean drag coefficient and Strouhal number of five rods. The average mean drag coefficient and Strouhal number are found to be decreased with an increment in the gap spacing. The results further show that as the value of gap spacing increases the average mean drag coefficient and Strouhal values almost approach to single rectangular rod value.

(iv) It is found that at small gap spacings the secondary rod interaction frequencies play an important role due to jet flow between rods. In case of large gap spacings the primary vortex shedding frequency is the dominant frequency and the secondary rod interaction frequencies diminish.

References

[1] A. Okajima, Strouhal numbers of rectangular cylinders, J. Fluid Mech. 123 (1982) 379–398.

[2] A. Sohankar, C. Norberg, L. Dvidson, Numerical simulation of unsteady low-Reynolds number flow around rectangular cylinders at incidence, J. Wind Eng. Ind. Aerodyn. 69 (1997) 189–201.

[3] B. Gera, P.K. Sharma, R.K. Singh, CFD analysis of 2D unsteady flow around a square cylinder, Int. J. Appl. Eng. Res., Dindigul 1 (3) (2010) 602–610.

[4] Y. Nakamura, Y. Ohya, R. Ozono, R. Nakayama, Experimental and numerical analysis of vortex shedding from elongated rectangular cylinders at low Reynolds numbers 200–10^3, J. Wind Eng. Ind. Aerodyn. 65 (1996) 301–308.

[5] S. Abdollah, A. Mahdi, R. Noorallah, Experimental study of near wake flow behind a rectangular cylinder, Am. J. Appl. Sci. 5 (2008) 917–926.

[6] A. Okajima, T. Nagahisa, A. Rpkugoh, A numerical analysis of flow around rectangular cylinders, Jpn. Soc. Mech. Eng. Ser II 33 (4) (1990).

[7] S.Ul. Islam, C.Y. Zhou, A. Shah, P. Xie, Numerical simulation of flow past rectangular cylinders with different aspect ratios using the incompressible lattice Boltzmann method, J. Mech. Sci. Technol. 26 (4) (2012) 1027–1041.

[8] M.M. Zdravkovich, Review of flow interference between two circular cylinders in various arrangements, Trans. ASME J. Fluids Eng. 99 (1977) 618–633.

[9] D. Sumner, S.S.T. Wong, S.J. Price, M.D. Paidoussis, Fluid behavior of side-by-side circular cylinders in steady cross-flow, J. Fluids Struct. 13 (1999) 309–339.

[10] M.M. Alam, Y. Zhou, Intrinsic features of flow around two side-by-side square cylinders, Phys. Fluids 25 (2013) 1–21.

[11] A. Agrawal, L. Djendi, R.A. Antonia, Investigation of flow around a pair of side-by-side square cylinders using the lattice Boltzmann method, Comput. Fluids 35 (2006) 1093–1107.

[12] S. Kang, Numerical study on laminar flow over three side-by-side cylinders, KSME Int. J. 18 (10) (2004) 1869–1879.

[13] H. Rahman, S.Ul. Islam, C.Y. Zhou, T. Kiyani, S.C. Saha, On the effect of Reynolds numbers for flow past three side-by-side square cylinders for unequal gap spacings, KSCE J. Civil Eng. 19 (1) (2014) 233–247.

[14] S.U. Islam, H. Rahman, C.Y. Zhou, S.C. Saha, Comparison of wake structures and force measurements behind three side-by-side cylinders, J. Braz. Soc. Mech. Sci. Eng. 38 (2016) 843–858.

[15] D.W. Guillaume, J.C. LaRue, Investigation of the flopping regime with two-, three- and four-cylinder arrays, Exp. Fluids 27 (1999) 145–156.

[16] Z. Huang, J.A. Olson, R.J. Kerekes, S.I. Green, Numerical simulation of the flow around rows of cylinders, Comput. Fluids 35 (2006) 485–491.

[17] S.D. Awale, Flow around row of four circular cylinders, J. Mater. Sci. Mech. Eng. 1 (1) (2014) 11–17.

[18] J. Mizushima, T. Akinaga, Vortex shedding from a row of square bars, Fluid Dyn. Res. 32 (2003) 179–191.

[19] S.R. Kumar, A. Sharma, A. Agarwal, Simulation of flow around a row of square cylinders, J. Fluid Mech. 606 (2008) 369–397.

[20] D. Chatterjee, G. Biswas, S. Amiroudine, Numerical simulation of flow past row of square cylinders for various separation ratios, Comput. Fluids 39 (2010) 49–59.

[21] D. Chatterjee, G. Biswas, Dynamic behavior of flow around rows of square cylinders kept in staggered arrangement, J. Wind Eng. Ind. Aerodyn. 136 (2015) 1–11.

[22] A.A. Mohamad, Lattice Boltzmann Method: Fundamentals and Engineering Applications with Computer Codes, Springer, 2011.

[23] D.A. Wolf-Gladrow, Lattice-Gas Cellular Automata and Lattice Boltzmann Models: An Introduction, Springer-Verlag, Berlin, Heidelberg, 2000.

[24] S. Chen, G. Doolen, Lattice Boltzmann method for fluid flows, Fluid Mech. 30 (1998) 329–364.

[25] M. Cheng, D.S. Whyte, J. Lou, Numerical simulation of flow around a square cylinder in uniform-shear flow, J. Fluids Struct. 23 (2) (2007) 207–226.

[26] D.P. Ziegler, Boundary conditions for lattice Boltzmann simulations, J. Stat. Phys. 71 (1993) 1171–1177.

[27] M.C. Sukop, D.T. Thorne Jr., Lattice Boltzmann Modeling: An Introduction for Geoscientists and Engineers, Springer, 2007.

[28] Y. Dazhi, M. Renwei, L.S. Luo, S. Wei, Viscous flow computations with the method of lattice Boltzmann equation, Prog. Aerosp. Sci. 39 (2003) 329–367.